

Systematic Analysis of Current Decay Time during Disruption in HYBTOK-II Tokamak

Masaaki OKAMOTO, Noriyasu OHNO¹⁾ and Shuichi TAKAMURA²⁾

Graduate School of Engineering, Nagoya University, Nagoya 464-8603, Japan

¹⁾*EcoTopia Science Institute, Nagoya University, Nagoya 464-8603, Japan*

²⁾*Faculty of Engineering, Aichi Institute of Technology, Toyota 470-0392, Japan*

(Received 24 October 2007 / Accepted 24 November 2007)

In order to estimate the electromagnetic force acting on vessel components during tokamak disruptions, an accurate prediction of the plasma current decay time is necessary. We have verified a current decay model based on a simple series circuit with a plasma resistance and an inductance. The circuit is employed for establishment of a plasma current decay time database using disruptive discharges in a small tokamak HYBTOK-II. An increase in the decay rate of the plasma current during the current quench phase was observed in experiments associated with an increase in the plasma resistance. This experimental result is consistent with the prediction of the model.

© 2008 The Japan Society of Plasma Science and Nuclear Fusion Research

Keywords: disruption, current quench, current decay rate, small tokamak

DOI: 10.1585/pfr.3.006

1. Introduction

The magnitude of damages to tokamak devices during disruptions must be estimated accurately in order to design tokamak fusion reactors. These disruptions are accompanied by an intense heat load on the divertor during thermal quench (TQ), and large electromagnetic (EM) forces on the vacuum vessel and in-vessel components because of eddy and halo currents induced during current quench (CQ). The eddy and halo currents are induced by the time variation of the plasma current and a vertical displacement event (VDE) [1], respectively. The EM forces, which are generated by the interaction between these currents and magnetic fields, could be large enough to mechanically break the in-vessel components [2]. In order to estimate the EM force generated by the eddy current, an accurate prediction of the plasma current decay time is crucial. In a recent study, we used a current decay model based on a simple series circuit of the plasma resistance R_p and inductance L_p to analyze the current decay time τ where τ_{model} can be described by L_p/R_p . The database for ITER (International Thermonuclear Experimental Reactor) [3] is established by using the current decay time τ normalized by the plasma cross-sectional area S . However, a few problems have been encountered; the data of the normalized τ exhibit large scattering among different tokamaks and operational shots. Therefore, it is strongly recommended that the validity of the current decay model be experimentally evaluated. In addition, this model must demonstrate that the normalized τ_{model} strongly depends on the plasma resistivity during CQ. In other words, it is important to accurately evaluate the electron temperature and effective charge during CQ. There have been only a few measurements of the

electron temperature during CQ in large and middle size tokamaks as it is difficult to perform measurements in these tokamaks because τ is very short, and the electron temperature is too low for the conventional diagnostic system in these devices to be measured during CQ. Electrostatic probes can measure the electron temperature during CQ. However, it is difficult to use the electrostatic probes in very hot plasma because the probe tips get severely damaged because of the enormous heat load during the disruptions. Therefore, the electron temperature is calculated using a numerical model, which is based on a power balance equation between joule heating and radiation loss because of impurity gases [4, 5].

On the other hand, probe measurements in the plasma can be performed at disruptive discharges in small tokamaks. Current density profiles and mode structures of MHD (Magnetohydrodynamics) instabilities at disruptive discharges have been reported by the magnetic probe measurement in the following devices: TOSCA [6, 7], LT-3 [8, 9], TBR-1 [10] and TORTUS [11]. However, the current decay time τ and electron temperature during CQ have not been reported for small tokamaks.

In this paper, the time evolution of the electron temperature during CQ is measured using a triple probe inserted into the small tokamak HYBTOK-II [12] and plasma resistivity is estimated by the classical Spitzer formula [13]. Simultaneously, the plasma internal inductance is estimated from the poloidal magnetic field, measured with the internal magnetic probe. This work aims to comprehensively verify the current decay model for establishment of the current decay time database using the obtained experimental data.

2. Model of Current Decay Time

If tokamak plasma is assumed to be represented by a simple series circuit consisting of resistance R_p and inductance L_p , loop voltage V_{loop} is expressed as

$$V_{loop} = \frac{d}{dt}(L_p I_p) + R_p I_p, \quad (1)$$

where I_p is the plasma current. If R_p and L_p are constant in time, and the absolute value of the right-hand side of Eq. (1) is much larger than the absolute value of V_{loop} , the temporal evolution of I_p can be expressed by the following equation:

$$I_p = I_{p0} \exp(-t/\tau_{model}), \quad (2)$$

where $\tau_{model} = L_p/R_p$ is the time constant of I_p decay, and I_{p0} is the plasma current before CQ. Equation (2) is valid when the current decay time is very short and plasma resistance is sufficiently large. When the current decay time can be approximated by $\tau_{model} = L_p/R_p$, the normalized current decay time τ_{model}/S can be expressed as

$$\frac{\tau_{model}}{S} = \frac{L_p/2\pi R_0}{\eta_p}, \quad (3)$$

where R_0 is the plasma major radius, η_p is the plasma resistivity, and $\eta_p = R_p S/2\pi R_0$. τ_{model}/S has little dependence on the device size, because L_p is approximately proportional to R_0 , and has a strong dependence on η_p , which is primarily determined by the electron temperature T_e and effective charge Z_{eff} in the classical Spitzer formula [13]. Thus, the database for ITER prediction is established in terms of the normalized current decay time τ/S [3]. However, R_p and L_p generally change in time, and occasionally the absolute values of the first and second terms in the right-hand side of Eq. (1) have a similar order of magnitude as V_{loop} . In this case, Eq. (3) cannot be valid. Therefore, to verify the current decay model, it is necessary to measure V_{loop} , L_p , and R_p in time during CQ experimentally.

3. Waveform of Disruptive Discharge in HYBTOK-II Tokamak

HYBTOK-II is a small standard tokamak with a circular cross-section of limiter configuration. The major radius R_0 is 40 cm, the minor radius of vacuum vessel a , and the limiter radius a_1 are 12.8 and 11 cm, respectively [12]. Figure 1 shows a typical waveform of a disruptive discharge in the HYBTOK-II. Zero in time corresponds to the initiating time of CQ. Disruption was driven by ramping up I_p to reduce the plasma surface safety factor $q_a (= aB_t/RB_\theta)$, where B_t and B_θ are the toroidal and poloidal magnetic field strengths, respectively [14, 15]. The typical parameters just before CQ are as follows: plasma minor radius is approximately 9.5 ~ 10.5 cm, $q_a \sim 3$, $I_p = 10$ -11 kA, and $B_t \sim 0.25$ T. It is found that the waveform of CQ consists of two phases of slow and fast current decays in

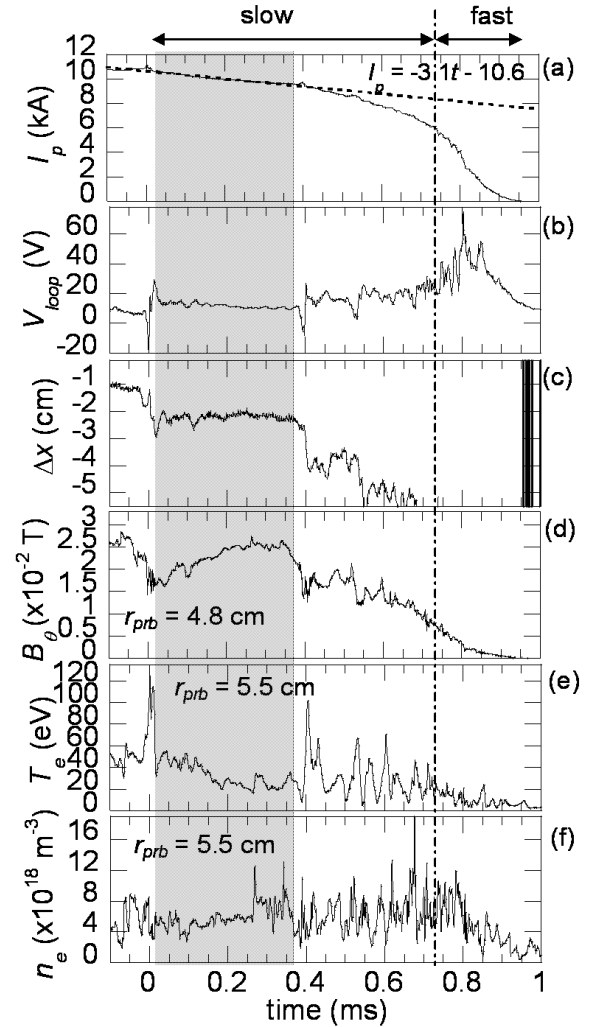


Fig. 1 Typical disruption waveform in HYBTOK-II ($B_t \sim 0.25$ T). Temporal evolutions of (a) plasma current I_p , (b) plasma loop voltage V_{loop} , (c) horizontal position of plasma center Δx , (d) poloidal magnetic field B_θ at $r_{prb} = 4.8$ cm and (e), (f) electron temperature T_e and density n_e at $r_{prb} = 5.5$ cm. The negative value of the plasma horizontal position corresponds to the high field side and $\Delta x = 0$ is the center of the vacuum vessel.

the HYBTOK-II disruptions as shown in Fig. 1 (a). In this paper, the current decay model is evaluated using a decay rate of I_p during the slow decay phase, because the plasma inductance and cross-sectional area can be experimentally obtained from the poloidal magnetic fields inside the plasma (Fig. 1 (d)) and the horizontal position of the plasma center from the center of vacuum vessel (Fig. 1 (c)), respectively. The electron temperature T_e is measured by a triple probe located at $r_{prb} = 5, 5.5,$ and 6 cm, and poloidal magnetic field B_θ is measured by a magnetic probe at $r_{prb} = 4.3, 4.8,$ and 5.3 cm, where r_{prb} is the distance between the central position of the vacuum vessel and each probe position. The probe and magnetic probe are inserted vertically along the minor radius from the bottom of the

vacuum vessel.

The time derivative of I_p , denoted by $\Delta I_p/\Delta t$, is determined by linear fitting during the initial phase of the slow decay, represented by a dashed line in Fig. 1 (a); here, $\Delta I_p/\Delta t$ becomes -3.1 kA/ms. The plasma inductance is evaluated from time-averaged values of B_θ and I_p over the hatched region in Fig. 1 on the basis of Ampere's Law with an assumption of the following current density profile [16]:

$$j(r) = j_0 \{1 - (r/a_p)^2\}^\nu. \quad (4)$$

Substituting Eq. (4) into the differential form of Ampere's law, $\mu_0 j = (1/r)d(rB_\theta)/dr$, B_θ can be expressed by the following equation:

$$B_\theta(r) = \frac{\mu_0 j_0 a_p^2}{2(\nu+1)} \frac{1 - \{1 - (r/a_p)^2\}^{\nu+1}}{r}, \quad (5)$$

where $a_p = a_1 + \Delta x$. Δx is the displacement of the center of the plasma column shown in Fig. 1 (c), and a_p is a plasma minor radius. The value of $B_\theta(a_p)$ can be calculated from the integral form of Ampere's Law, $B_\theta(a_p) = \mu_0 I_p / 2\pi a_p$, using the measured value of I_p . Peaking factor ν in Eq. (5) can be determined by $B_\theta(a_p)$ and $B_\theta(r_p)$, where $r_p = \sqrt{\Delta x^2 + r_{prb}^2}$. Therefore, the plasma inductance L_p can be calculated from

$$l_i = \frac{\overline{B_\theta(r)^2}}{B_\theta(a_p)^2} = \frac{2 \int_0^{a_p} B_\theta(r)^2 r dr}{a_p^2 B_\theta(a_p)^2}, \quad (6)$$

$$L_p = \mu_0 R_0 \left(\frac{l_i}{2} + \ln \frac{8R_0}{a_p} - 2 \right). \quad (7)$$

Time-averaged I_p and B_θ over the hatched region in Fig. 1 give $\langle \nu \rangle = 1.56$, $\langle l_i \rangle = 1.09$, and $\langle L_p \rangle = 1.0 \mu\text{H}$, where $\langle \rangle$ indicates that the values are time-averaged. Therefore, $|\langle L_p \rangle \Delta I_p / \Delta t|$ can be estimated to be 3.1 V, which is in the same order of magnitude as the time-averaged V_{loop} of 11.7 V. It is found that Eqs. (2) and (3) cannot be used during the slow decay phase in Fig. 1 (a), therefore, we need to verify Eq. (1) directly.

4. Verification of Current Decay Model Based on a Simple Series Circuit

We have analyzed 115 disruptive shots. Figure 2 shows a histogram of $\langle T_e \rangle$ taken among these 115 disruptive shots. $\langle T_e \rangle$ indicates the time-averaged value of T_e during the slow decay phase. T_e is measured at different radial positions, $r_{prb} = 5, 5.5,$ and 6 cm. The $\langle T_e \rangle$ has little dependence on the radial position because the radial profile of T_e is flat. However, a large variation of $\langle T_e \rangle$ among the disruptive shots appears even at the same radial position. The large variation could be caused by a difference in the particle recycling rate because of inward shift of the plasma column. We can verify Eq. (1) at range of $\langle T_e \rangle$ from about 30 to 50 eV.

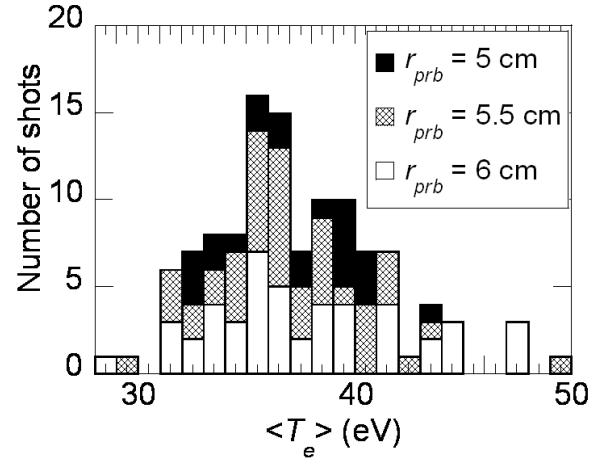


Fig. 2 Histogram of time-averaged electron temperature $\langle T_e \rangle$ during the slow decay phase.

In order to evaluate the validity of Eq. (1), we need to estimate the plasma resistivity in the hatched region during slow decay phase of CQ. The plasma resistivity can be calculated using the classical Spitzer formula [13],

$$\eta_p = 1.65 \times 10^{-9} Z_{\text{eff}} T_e^{-3/2} \ln \Lambda, \quad T_e \text{ in keV} \quad (8)$$

where Z_{eff} and $\ln \Lambda$ are the effective charge and Coulomb logarithm, respectively. There are two methods to calculate the time-averaged plasma resistivity $\langle \eta_p \rangle$ over the hatched region. A simple method is to calculate $\langle \eta_p \rangle$ by substituting $\langle T_e \rangle$ into Eq. (8), referred to as $\eta_p(\langle T_e \rangle)$. In another method, after calculating the time evolution of $\eta_p(t)$ by substituting T_e in Eq. (8) by the T_e value shown in Fig. 1 (e), $\langle \eta_p \rangle$ is calculated by averaging $\eta_p(t)$ over the hatched region in Fig. 1, and $\langle \eta_p \rangle$ is denoted by $\langle \eta_p(T_e) \rangle$. In general, $\langle \eta_p(T_e) \rangle$ becomes larger than $\eta_p(\langle T_e \rangle)$ because of the nonlinear dependence of $\eta_p \propto T_e^{-3/2}$. Figure 3 shows the comparison between $\eta_p(\langle T_e \rangle)$ and $\langle \eta_p(T_e) \rangle$ at $Z_{\text{eff}} = 1$. It is found that $\langle \eta_p(T_e) \rangle$, calculated by the temporal evolution of T_e , becomes larger than $\eta_p(\langle T_e \rangle)$ calculated by time-averaged value of T_e . This indicates that the measurement of electron temperature with good time resolution is important for estimating the precise plasma resistance to evaluate the current decay model. We will use the values of $\langle \eta_p(T_e) \rangle$ hereafter.

If R_p and L_p are constant, using Eq. (1), the rate of I_p decay can be expressed as

$$\frac{dI_p}{dt} = \frac{-I_p R_p + V_{loop}}{L_p}. \quad (9)$$

Figure 4 shows the time-averaged values of plasma inductance, loop voltage, and plasma current as functions of the time-averaged value of $T_e^{3/2}$. Because $\langle T_e^{3/2} \rangle$ varies from approximately 100 to 300 among the shots, it seems that $\langle \eta_p \rangle$ varies by approximately three times of that evaluated

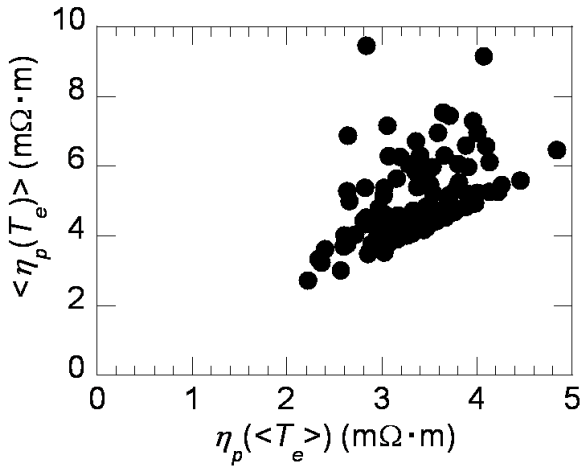


Fig. 3 Comparison between $\langle \eta_p(T_e) \rangle$ and $\eta_p(\langle T_e \rangle)$. $\langle \eta_p(T_e) \rangle$ is calculated by $\eta_p(t)$ averaging over the hatched region in Fig. 1. $\eta_p(\langle T_e \rangle)$ is calculated by time-averaged $\langle T_e \rangle$ over the hatched region in Fig. 1.

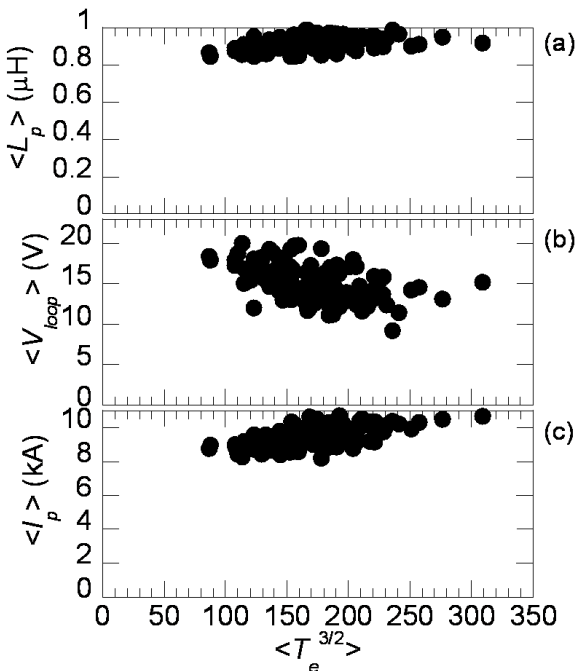


Fig. 4 Time-averaged values of (a) plasma inductance L_p , (b) loop voltage V_{loop} , and (c) plasma current I_p during the slow decay phase, as a function of the time-averaged value of $T_e^{3/2}$.

by Eq. (8). Both $\langle L_p \rangle$ and $\langle I_p \rangle$ slightly increase with $\langle T_e^{3/2} \rangle$. On the other hand, $\langle V_{loop} \rangle$ decreases with $\langle T_e^{3/2} \rangle$; however, although $\langle T_e^{3/2} \rangle$ varies by approximately three times, $\langle V_{loop} \rangle$ changes only twice. We speculate that the variation of I_p decay rate is primarily determined by the change in plasma resistance among the shots from Eqs. (8) and (9).

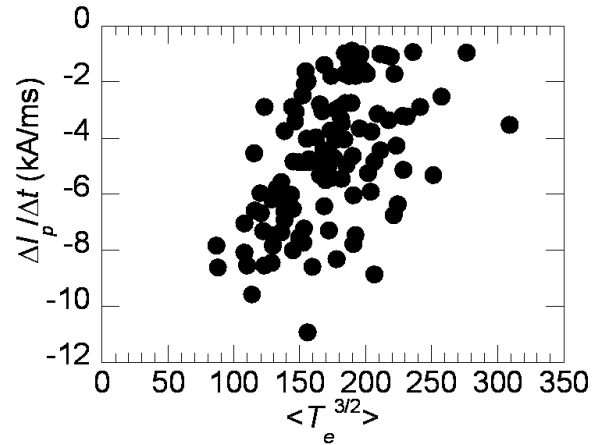


Fig. 5 Decay rate of the plasma current decay I_p during the slow decay phase as a function of $\langle T_e^{3/2} \rangle$.

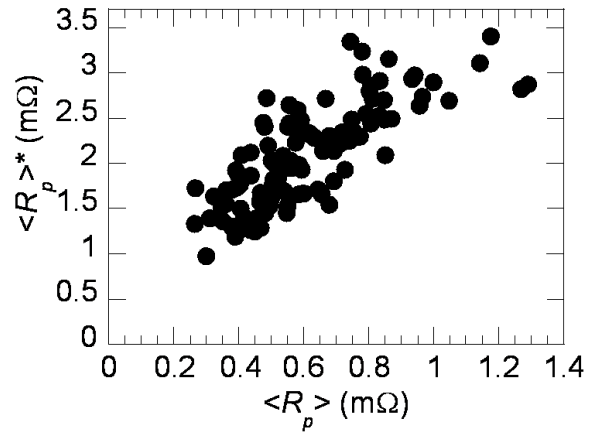


Fig. 6 Plasma resistance $\langle R_p \rangle^*$ calculated from a circuit equation using experimental values of $\Delta I_p / \Delta t$, $\langle L_p \rangle$, $\langle I_p \rangle$ and $\langle V_{loop} \rangle$ versus plasma resistance $\langle R_p \rangle$ calculated by the Spitzer formula with the assumption of $Z_{eff} = 1$.

Figure 5 shows the rate of I_p decay $\Delta I_p / \Delta t$ as a function of $\langle T_e^{3/2} \rangle$. It is found that $\Delta I_p / \Delta t$ increases with an increase in $\langle T_e^{3/2} \rangle$ associated with the change in plasma resistance. This experimental result is in qualitative agreement with the prediction from Eq. (9); however it is not quantitatively consistent. In order to make a quantitative comparison between the experimental results and Eq. (9), we compare the plasma resistances evaluated by two calculation methods. One, which is denoted by $\langle R_p \rangle$, is calculated from Eq. (8) using experimental values of $\langle T_e^{3/2} \rangle$ and the assumption of $Z_{eff} = 1$. The other, which is denoted by $\langle R_p \rangle^*$, is calculated from Eq. (9) using experimental values of $\Delta I_p / \Delta t$, $\langle L_p \rangle$, $\langle I_p \rangle$, and $\langle V_{loop} \rangle$. Figure 6 shows a comparison between $\langle R_p \rangle$ and $\langle R_p \rangle^*$. It is found that $\langle R_p \rangle^*$ increases with $\langle R_p \rangle$; however, $\langle R_p \rangle^*$ is much larger than $\langle R_p \rangle$,

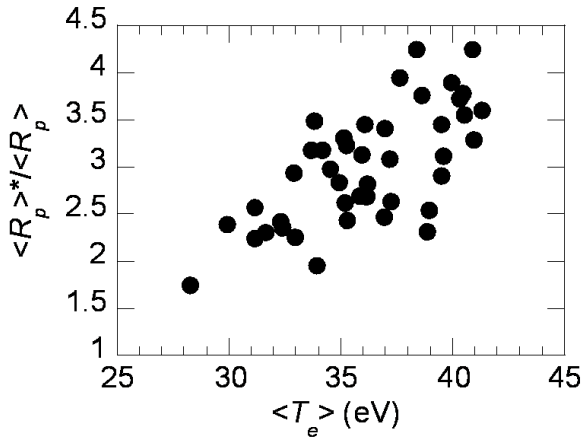


Fig. 7 Ratio between plasma resistance $\langle R_p \rangle$ calculated by the Spitzer formula with $Z_{\text{eff}} = 1$, and $\langle R_p \rangle^*$ calculated by a circuit equation using experimental values of $\Delta I_p / \Delta t$, $\langle L_p \rangle$, $\Delta L_p / \Delta t$, $\langle I_p \rangle$, and $\langle V_{\text{loop}} \rangle$ as a function of the time-averaged electron temperature $\langle T_e \rangle$.

even if the term $\Delta L_p / \Delta t$ is considered in the plasma resistance calculation using a circuit equation. Figure 7 shows the ratios of $\langle R_p \rangle^*$ to $\langle R_p \rangle$ as a function of $\langle T_e \rangle$. The ratio of $\langle R_p \rangle^*$ to $\langle R_p \rangle$ increases monotonically with $\langle T_e \rangle$. This result could suggest that the effective charge Z_{eff} increases with $\langle T_e \rangle$ in the experiments, although Z_{eff} is assumed to be unity in our calculation. Unfortunately, there are no experimental data for Z_{eff} at this moment, but the discrepancy between $\langle R_p \rangle^*$ and $\langle R_p \rangle$ will be discussed in the next section.

5. Discussion

In our experiment, the working gas is hydrogen. The limiter and vacuum vessel are made of molybdenum and stainless steel, respectively. If the electron temperature dependence of the ratio of $\langle R_p \rangle^*$ to $\langle R_p \rangle$ in Fig. 7 is determined by the variation of Z_{eff} , then Z_{eff} should vary from 2 to 4.5 in the range of electron temperature from 28 to 42 eV. With 1% iron impurity in the plasma, Z_{eff} could be varied from 1.25 to 1.33 at an electron temperature from 28 to 42 eV. In this analysis, we have used the ionization states of iron calculated by Arnaud and Rothenflug [17]. In Ref. [17], the main ionization states of iron are the fifth and sixth charged states at $T_e = 28$ eV, and are the sixth and seventh charged states at $T_e = 42$ eV. Specific numerical values are as follows: $n_{\text{Fe}+3} : n_{\text{Fe}+4} : n_{\text{Fe}+5} : n_{\text{Fe}+6} : n_{\text{Fe}+7} : n_{\text{Fe}+8} = 0.001 : 0.057 : 0.43 : 0.38 : 0.12 : 0.004$ at $T_e = 28$ eV and $n_{\text{Fe}+4} : n_{\text{Fe}+5} : n_{\text{Fe}+6} : n_{\text{Fe}+7} : n_{\text{Fe}+8} : n_{\text{Fe}+9} = 0.008 : 0.13 : 0.42 : 0.35 : 0.091 : 0.001$ at $T_e = 42$ eV. The assumption of 1% iron impurity in plasma is insufficient to explain the discrepancy. However, we should measure the value of Z_{eff} experimentally in the future in order to form a more comprehensive discussion. Another possibility to explain the dis-

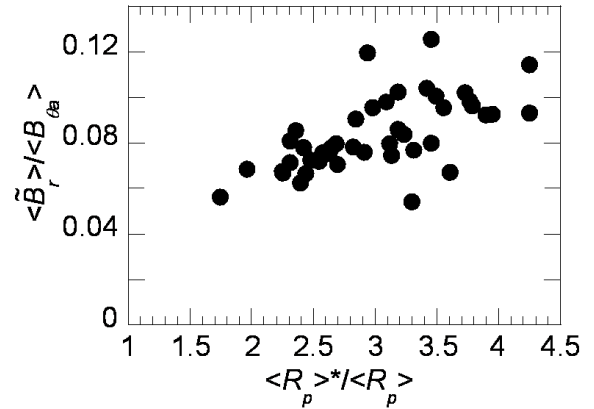


Fig. 8 Normalized amplitude of the spontaneous radial magnetic field fluctuation as a function of $\langle R_p \rangle^* / \langle R_p \rangle$. $B_{\theta a}$ is the poloidal magnetic field at the plasma surface.

crepancy is the anomalous resistivity because of magnetic fluctuations associated with magnetic field line reconnection [18]. In Ref. [18], detailed experiments on this anomalous resistivity were performed by Stenzel and Gekelman within a comparatively large facility (1 m in diameter, 2 m long). A rarefied plasma was produced at plasma density of 10^{12} cm^{-3} with an electron temperature of approximately 10 eV. They reported the increase of the plasma resistivity by two orders of magnitude because of anomalous electron scattering. Figure 8 shows the normalized amplitude of magnetic fluctuation of the internal radial magnetic field B_r as a function of the ratio of $\langle R_p \rangle^*$ and $\langle R_p \rangle$. It is found that the amplitude of internal magnetic fluctuation increases with this ratio. This could suggest that the plasma resistivity may be influenced by anomalous resistivity induced by magnetic fluctuations associated with MHD instability.

6. Summary

We have verified the current decay model to establish a database of the current decay time using the slow decay phase of HYBTOK-II disruptive discharges. It is experimentally confirmed that the decay rate of the plasma current during the current quench becomes quicker with an increase in the plasma resistance, which is consistent with the current decay model. The discrepancy in plasma resistivities, estimated from the current decay model and calculated by the classical Spitzer formula, is discussed based on the effective charge in plasma and anomalous resistivity associated with magnetic perturbation. In order to evaluate the model more accurately in the future, direct measurement of the effective charge in the plasma is necessary.

Acknowledgments

We acknowledge the technical support provided by Mr M. Takagi in Nagoya University. This work was par-

tially supported by the Grant-in-Aid for Scientific Research from the Japan Society for the Promotion of Science (JSPS) Research Fellowships for Young Scientists (No. 19-8456).

- [1] R.O. Sayer, Y.K.M. Peng, S.C. Jardin, A.G. Kellman and J.C. Wesley, *Nucl. Fusion* **33**, 969 (1993).
- [2] K. Masaki, T. Ando, K. Kodama, T. Arai *et al.*, *J. Nucl. Mater.* **220-222**, 390 (1995).
- [3] Progress in the ITER Physical Basis, *Nucl. Fusion* **47**, S171 (2007).
- [4] H. Ohwaki, M. Sugihara and A. Hatayama, *Plasma Fusion Res.* **1**, 016 (2006).
- [5] M. Bakhtiari and D.G. Whyte, *Phys. Plasmas* **13**, 112511 (2006).
- [6] D.C. Robinson and K.M. McGuire, *Nucl. Fusion* **19**, 115 (1979).
- [7] K.M. McGuire and D.C. Robinson, *Phys. Rev. Lett.* **44**, 1666 (1980).
- [8] I.H. Hutchinson, *Phys. Rev. Lett.* **37**, 338 (1976).
- [9] A.H. Morton, *Nucl. Fusion* **16**, 571 (1976).
- [10] A. Vannucci, I.C. Nascimento and I.L. Caldas, *Plasma Phys. Control. Fusion* **31**, 147 (1989).
- [11] L. Giannone, R.C. Cross and I.H. Hutchinson, *Nucl. Fusion* **27**, 2085 (1987).
- [12] S. Takamura, Y. Kikuchi, Y. Uesugi and M. Kobayashi, *Nucl. Fusion* **43**, 393 (2003).
- [13] L. Spitzer and R. Härm, *Phys. Rev.* **89**, 977 (1953).
- [14] M. Okamoto, T. Yamada, T. Hiraishi, Y. Kikuchi, N. Ohno and S. Takamura, *J. Nucl. Mater.* **363-365**, 1076 (2007).
- [15] M. Okamoto, S. Takamura, N. Ohno, S. Kajita, Y. Kikuchi, Y. Uesugi, T. Ozeki, Y. Kawano and M. Sugihara, *Nucl. Fusion* **47**, 1106 (2007).
- [16] J.A. Wesson, *Tokamaks* 3rd edition (New York: Oxford University Press, 2004) chapter 3.
- [17] M. Arnaud and R. Rothenflug, *Astron. Astrophys. Suppl. Ser.* **60**, 425 (1985).
- [18] N. Wild, W. Geckelman and R.L. Stenzel, *Phys. Rev. Lett.* **46**, 339 (1981).